Smart Structures and Systems, *Vol. 25, No. 1* (*2020*) *81-96*
DOI: https://doi.org/10.12989/sss.2020.25.1.081

Wind-induced responses and dynamic characteristics of a super-tall building under a typhoon event

X.G. Hua*[1], K. Xu [1a], Y.W. Wang [2b], Q. Wen [3c] and Z.Q. Chen [1d]

[1] *Key Laboratory for Wind and Bridge Engineering of Hunan Province*, *College of Civil Engineering*, *Hunan University*, *410082 Changsha*, *Hunan*, *China*
[2] *Department of Civil and Structural Engineering*, *Hong Kong Polytechnic University*, *Kowloon*, *Hong Kong SAR*, *China*
[3] *Hunan Provincial Key Laboratory of Structural Engineering for Wind Resistant and Vibration Control*, *Hunan University of Science and Technology*, *411201*, *Xiangtan*, *China*

(*Received December 1, 2018, Revised October 8, 2019, Accepted October 13, 2019*)

Abstract. Wind measurements were made on the Canton Tower at a height of 461 m above ground during the Typhoon *Vincente*, the wind-induced accelerations and displacements of the tower were recorded as well. Comparisons of measured wind parameters at upper level of atmospheric boundary layer with those adopted in wind tunnel testing were presented. The measured turbulence intensity can be smaller than the design value, indicating that the wind tunnel testing may underestimate the crosswind structural responses for certain lock-in velocity range of vortex shedding. Analyses of peak factors and power spectral density for acceleration response shows that the crosswind responses are a combination of gust-induced buffeting and vortex-induced vibrations in the certain range of wind directions. The identified modal frequencies and mode shapes from acceleration data are found to be in good agreement with existing experimental results and the prediction from the finite element model. The damping ratios increase with amplitude of vibration or equivalently wind velocity which may be attributed to aerodynamic damping. In addition, the natural frequencies determined from the measured displacement are very close to those determined from the acceleration data for the first two modes. Finally, the relation between displacement responses and wind speed/direction was investigated.

Keywords: field measurements; wind characteristics; crosswind responses; modal identification; Canton Tower

1. Introduction

Wind engineering studies are very important for design of super-tall buildings, especially for those located in tropical storm-prone regions. Wind tunnel testing is the main tool for performing such studies to determine wind environments and their static/dynamic actions on building structures (Holmes 2001, Irwin 2008), which can be further validated by full-scale measurements. Due to uncertainty in design parameters (such as wind and structural parameters) and lack of modeling in Reynolds number, significant deviations between wind tunnel tests and full-scale measurements may arise (Davenport 1975). Field measurements are also important for improved modeling of wind-field characteristics (e.g., Ye *et al*. 2018), verification of quasi-steady assumption (Banks and Meroney 2001, Caracoglia and Jones 2009), improved understanding of structural damping (Tamura and Suganuma 1996), and structural vibration control (Kareem *et al*. 1999, Bortoluzzi *et al*. 2015, Lu *et al*. 2016, Sun *et al*. 2019).

During the past two decades, measurement techniques have greatly evolved as a result of advancement in instrumentations and data processing (e.g., Brownjohn 2007). Numerous full-scale measurements of wind effects on tall buildings have been made throughout the world. Porterfield and Jones (2001) reported the measurement campaign on collected meteorological, pressure, strain and displacement data on a low-rise structure during 1997-2001. Xu and Zhan (2001) measured wind and structural response on the 384 m-high Di Wang Tower (Shenzhen, China) during Typhoon York in 1999. Tamura *et al*. (2002) measured displacements by RTK-GPS for three tall buildings which provided both the dynamic components and static components, and the dynamic components are shown in good agreement with accelerations. Campbell *et al*. (2005) analyzed dynamic responses of two residential buildings in Hong Kong and the results indicated wind-induced responses of the two buildings for two typhoon events follow a Gaussian distribution. Kijewski-Correa *et al*. (2006) reported the field measurement on three Chicago tall buildings undertaken by Notre Dame University, some further results were described by Bashor *et al*. (2012). Brownjohn and Pan (2008) conducted long-term monitoring for a 280 m-high office tower in Singapore by installing a pair of tri-component propeller anemometers together with strain gauges and accelerometers, with the purpose of identifying loading and response mechanisms. Li and his

*Corresponding author, Professor,
E-mail: cexghua@hnu.edu.cn
[a] Ph.D. Student, E-mail: kaixu@hnu.edu.cn
[b] Ph.D., E-mail: yw.wang@connect.polyu.hk
[c] Ph.D., Assistant Professor, E-mail: cewenq@hnust.edu.cn
[d] Ph.D., Profesor, E-mail: zqchen@hnu.edu.cn

ISSN: 1738-1584 (Print), 1738-1991 (Online)

colleagues made comprehensive field measurements for several high-rise buildings under strong winds (e.g., Li *et al*. 2004, 2018). Based on the measurement data, the authors have studied some relevant issues including the identification of amplitude-dependent damping and the comparison with wind tunnel test results. Au *et al*. (2012) investigated the modal properties of two tall buildings under strong wind. Siringoringo and Fujino (2017) measured the dynamic response of a base-isolated tall building and revealed that its responses are dominated by the first mode. As the typhoons are often non-stationary, nonstationary analysis on the wind characteristics of a tropical storm have also been reported (e.g., Tao *et al*. 2016). Upper level wind parameters over the nominal gradient height (350 m-450 m above ground) are very important for wind resistant design of super-tall buildings (Irwin 2009), however they are seldom reported in the literature (He *et al*. 2018).

The Canton Tower situated in the city of Guangzhou, China, is a 610 m-high super tall building. Guangzhou is located in the coastal areas which are frequently attacked by typhoon during summer seasons. Due to its extreme flexibility and unusual aerodynamic shape, great attentions have been paid on wind tunnel studies of the tower, which involve in pressure and aerodynamic force tests of partial and full tower, and aeroelastic model test of the full tower. Additionally, a sophisticated long-term structural health monitoring (SHM) system consisting over 700 sensors has been implemented in the Canton Tower for real-time monitoring at both in-construction and in-service stages (Ni *et al.* 2009). Pertinent information such as wind conditions, and structural responses can be acquired in real time. This paper reports the measured wind characteristics at elevation 461m above ground and structural responses of the Canton Tower during Typhoon *Vincente*. Implications of measured wind characteristics and their impact on wind tunnel testing are discussed.

Fig. 1 Canton Tower

2. Description of Canton Tower and monitoring system

The Canton Tower located in the city of Guangzhou, China, is a super-tall structure with a total height of 610 m, which includes a main tower and a mast above. The main tower is 454 m high and comprises an interior reinforced concrete (RC) column structure surrounded by an exterior latticed steel frame with helical shape. The interior column has a constant ellipse cross-section of 14×17 m, while the geometric configuration of the exterior frame varies with height, which decreases from 50 m×80 m at the ground level to the minimum of 20.7 m×27.7 m at the height of 280 m (waist level), and then increases to 41 m×55 m at the very top of the main tower (454 m). There are 37 unevenly-distributed floors connecting the interior RC column and exterior steel frame that serve for various functions including TV and radio transmission facilities, observatory decks, revolving restaurants, exhibition spaces, conference rooms, shopping malls and 4D cinemas. The mast reaching 164 m high above the tower top is a latticed steel structure with an octagonal cross-section of 14 m in the maximum diagonal. Fig. 1 shows the overview of the Canton Tower. Fig. 2 shows the location of the Canton Tower and surrounding terrain conditions.

Fig. 2 Location of Canton Tower and surrounding terrain conditions

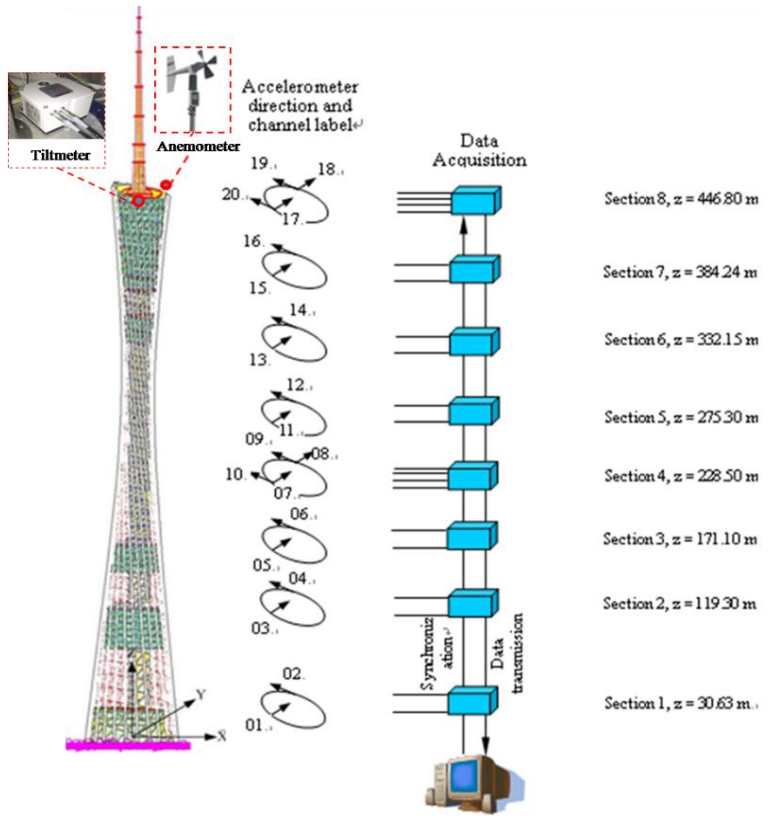

Fig. 3 Deployment of accelerometers and the data acquisition system

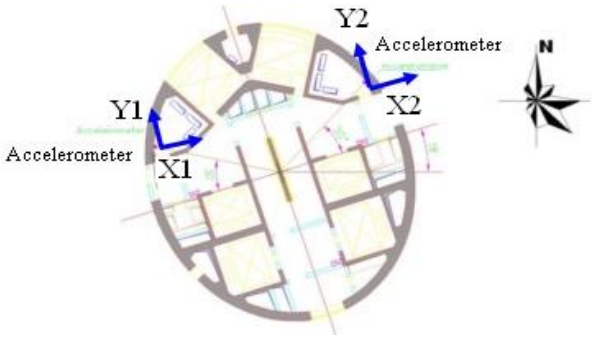

Fig. 4 Layout of accelerometers in a horizontal plane

A sophisticated long-term SHM system consisting over 700 sensors has been implemented in the Canton Tower (Ni *et al*. 2009). The sensors relevant to this study are accelerometers, anemometers and tiltmeters. Twenty uni-axial accelerometers (Tokyo Sokushin, AS-2000C) were installed at eight levels (at height of 30.6 m, 119.3 m, 171.1 m, 228.5 m, 275.3 m, 332.2 m, 384.2 m and 446.8 m) of the interior RC column to monitor the acceleration responses, as shown in Fig. 3. The 4th level and 8th level are equipped with four uni-axial accelerometers, two for the horizontal acceleration along the short-axis of the RC column (X1 and X2 shown in Fig. 4), and the other two for the long-axis (Y1 and Y2 shown in Fig. 4). The other six levels, each cross-section was equipped with two uni-axial accelerometers, one along the short-axis of the RC column, and the other along the long-axis. The frequency range of accelerometers is DC-50Hz, the amplitude range is ±2 g, and the sensitivity is ±1.25 v/g. One anemometer (R.M Youngh, 05103 L) is installed at the height of 461 m above ground. The anemometer is calibrated that 0° denotes north direction and an arbitrary direction is measured from north in a clockwise direction. The wind speed range is 0~100 m/s, wind direction is 0~360° and the sampling frequency is 50Hz. One bi-axial tiltmeter (Leica Geosvstems, NIVEL210) is installed at the height of 443.6 m. The measurement range is ±3 mill-rad, the sensitivity is 0.001 mill-rad and the sampling frequency is 1 Hz.

3. Description of wind characteristics

3.1 Typhoon Vincente

The tropical storm *Vincente* formed over the western North Pacific about 460 kilometers northeast of Manila on 20th July 2012 and moved west-northwestwards (Hong Kong Observatory 2012). *Vincente* began to edge towards the south China coast to the west of the Pearl River Estuary on 23 July and underwent rapid intensification to typhoon in the afternoon and further to a severe typhoon around mid-night, reaching its peak intensity with an estimated maximum sustained wind of 155 km/h near its centre. *Vincente* made landfall near the coastal areas of Taishan, Guangdong, where is 133 km from the Canton Tower, at 4:15 on 24 July, with minimum central pressure of 955 hPa and maximum sustained wind of 144 km/h near its centre. It subsequently moved generally west-northwest across western Guangdong and Guangxi and weakened gradually.

Fig. 5 Moving tracks of Typhoon Vincente

Vincente dissipated over the northern part of Vietnam on 25 July. Fig. 5 shows the moving tracks of Typhoon *Vincente*.

3.2 Mean wind speed and wind direction

The wind speed and wind direction are recorded by propeller anemometer located atop of the main tower at an elevation of 461 m above ground. Fig. 6 illustrates some typical measurement data for 10-minite duration. It can be seen that the wind velocity is still rather fluctuating. The measurement data for each 10-minite interval are analyzed to derive wind characteristics. For each measurement data of 10-minite interval, the wind velocity is first decomposed into two orthogonal directions in a plane, namely x and y directions as shown in Fig. 7(a), as follows

$$\begin{aligned} u_x(t) &= \tilde{u}(t)\cos\theta(t) \\ u_y(t) &= \tilde{u}(t)\sin\theta(t) \end{aligned} \tag{1}$$

where $\tilde{u}(t)$ and $\theta(t)$ are the measured instantaneous wind speed and the measured instantaneous wind direction at time instant t, respectively.

The alongwind mean wind speed $\bar{U}$ and the principal direction ϕ for each 10-minite duration, as defined in Fig. 7(b), are then determined as

$$\begin{aligned} \bar{U} &= \sqrt{\bar{u}_x^2 + \bar{u}_y^2} \\ \phi &= arctan(\bar{u}_y/\bar{u}_x) \end{aligned} \tag{2}$$

where $\bar{u}_x$, $\bar{u}_y$ are the mean values of data series $u_x(t_i)$ and $u_y(t_i)$, respectively.

The fluctuating longitudinal and crosswind components of wind speed, $u(t)$ and $v(t)$ are then obtained as

$$\begin{aligned} u(t) &= u_x(t)\cos\phi + u_y(t)\sin\phi - \bar{U} \\ v(t) &= -u_x(t)\sin\phi + u_y(t)\cos\phi \end{aligned} \tag{3}$$

Fig. 8 shows the variation of the 10-minite mean wind speed and wind direction at main tower top during Typhoon *Vincente*. It is seen that the wind speed increased gradually from the 23:00 on 23 July, reaching the peak (the maximum 10-minite wind speed is 30.2 m/s) at about 4:00 on 24 July, at this moment *Vincente* made landfall, and then steadily decreased. The wind direction varies significantly during Typhoon *Vincente*.

3.3 Turbulence intensity

Turbulence intensity characterizes the intensity of gusts in the flow. It is an important parameter that can strongly affect the dynamic responses of buildings and structures to wind. For turbulence-induced buffeting, larger turbulence intensity gives rise to increased dynamic responses. On the contrary, for crosswind responses due to vortex excitation, smaller turbulence intensity leads to larger dynamic responses since more coherent vortices are generated for smaller turbulence (Irwin 2009).

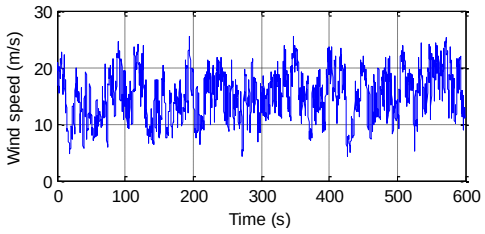

(a) Wind velocity

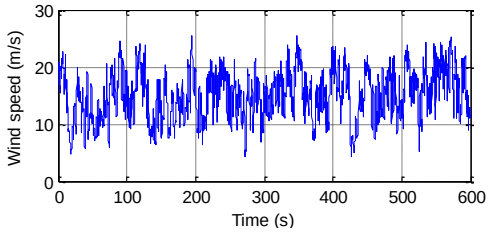

(b) Wind direction

Fig. 6 10-minute measurement data of wind at main tower top

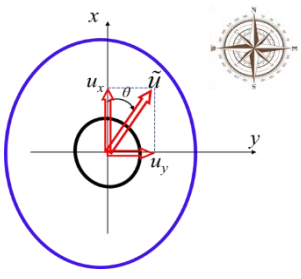

(a) Instantaneous wind

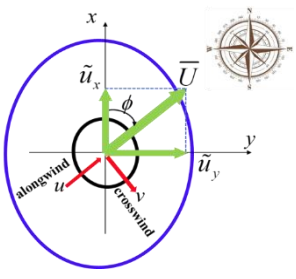

(b) Alongwind and crosswind component

Fig. 7 Definition of wind speed and wind direction

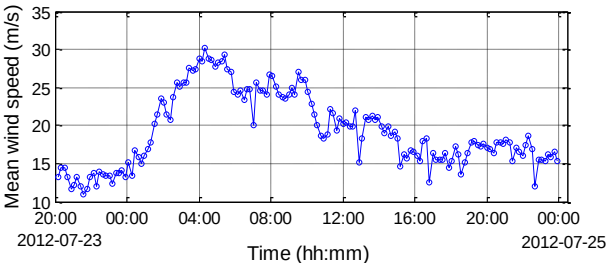

(a) Wind speed

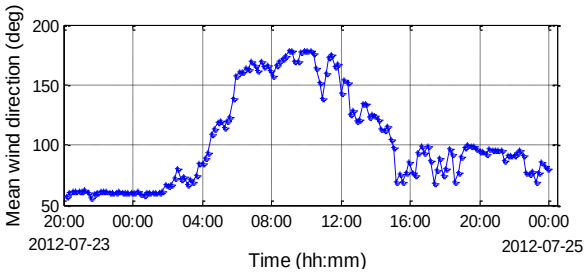

(b) Wind direction

Fig. 8 Variations of mean wind speed and wind direction

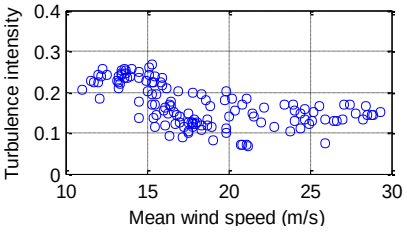

(a) Longitudinal

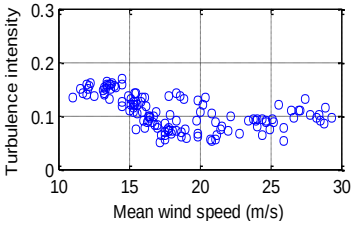

(b) Lateral

Fig. 9 Variation of turbulence intensity with mean wind speed

The turbulence intensities in longitudinal, lateral and vertical directions are defined as

$$I_i = \frac{\sigma_i}{\overline{U}} (i = u, v, w) \tag{4}$$

where $\sigma_i (i = u, v, w)$ are the root mean square (RMS) value of the fluctuating wind speed component in longitudinal, lateral and vertical directions, respectively; $\bar{U}$ is the mean wind speed. For wind measurements from propeller anemometers, only longitudinal and lateral components are available.

While the measured maximum wind velocity is well below the design wind velocity (52.4 m/s at main tower top), it is still worth to compare the measured turbulence intensity with that adopted in wind tunnel testing or existing measurement data. Fig. 9 shows the variations of the longitudinal and lateral turbulence intensities with mean wind speed. There is a tendency of decreasing turbulence intensity with wind speed for both directions, and the average turbulence intensities in longitudinal and lateral directions are 0.13 and 0.10, respectively for wind velocity above 15 m/s. During wind tunnel tests, a value of 0.1 has been adopted (Zhu *et al*. 2006), which is very close to the value recommended by the Architectural Institute of Japan (AIJ 1996). According to the ASCE7 (ASCE 2006), the turbulence intensity is 0.16. It is found that the measured longitudinal turbulence intensity is larger than that given in AIJ, but smaller than that given in ASCE7. Li and his co-investigators have made full-scale measurements for several high-rise buildings under strong winds and obtained many results on turbulence intensity: the average turbulence intensities in longitudinal and lateral directions measured from atop CPT (at height of 350 m) during Typhoon Sanvu are 0.11 and 0.09, respectively; the average values of longitudinal and lateral turbulence intensity measured from atop DWT (at height of 345 m) during typhoon are 0.19 and 0.11, respectively; the average value of longitudinal measured from atop DWT during Typhoon Sally is 0.12. It can be found that the turbulence intensity varies for different wind events.

On the other hand, as shown in Fig. 9, the minimum longitudinal turbulence intensity reaches only about 0.07, which is smaller than that given in design codes. It is well known that the crosswind responses can be contributed both by wind buffeting from turbulence as well as by vortex-induced vibration from vortex excitations. Moreover, at low velocity range, the contribution from vortex-induced vibration can be even higher than that from wind buffeting (Irwin 2009). Larger turbulence intensity adopted in wind tunnel testing may suppress the vortex-induced vibrations which otherwise may occur at actual buildings subjected to wind flow with smaller turbulence intensity. In this regard, wind tunnel tests based on the code-specified turbulence intensity may underestimate the crosswind responses for certain wind velocity range of vortex shedding. As such, it is very important to cover all the potential parameter ranges when evaluating dynamic responses for wind tunnel tests.

The Canton Tower (CT) is the highest building in Canton City. Its surrounding terrain condition is shown in Fig. 2. In the north of the tower, it is surrounded by a great amount of the tall buildings with heights of less than 150 m. In particular, there are a number of high-rise buildings, such as Zhoudafu Financial Center (ZFC), which is height of 530 m and is 1.3 km away from the Canton Tower, and Canton International Financial Center (IFC), which is height of 441 m and 1.3 km away from the Canton Tower. The building height in the south of the tower is relatively below 100 m. Fig. 10 shows the variations of the longitudinal and lateral turbulence intensities with mean wind direction. The prevailing wind direction at the Canton Tower during Typhoon *Vincente* varies from northwest clockwise to southeast. Therefore, the turbulence intensity does not change considerably with the mean wind direction as shown in Fig. 10, as high-rise buildings are mainly located on the north of the Canton Tower.

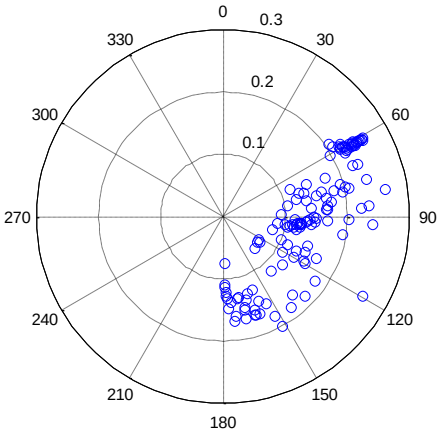

(a) Longitudinal

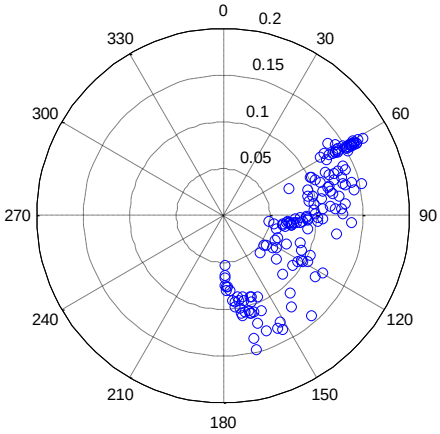

(b) Lateral

Fig. 10 Turbulence intensity versus wind direction

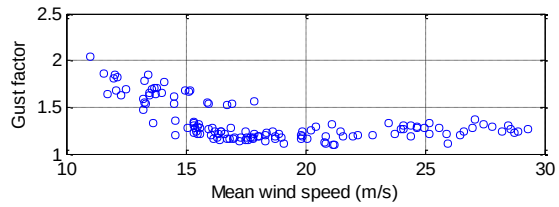

(a) Variation of gust factor with mean wind velocity

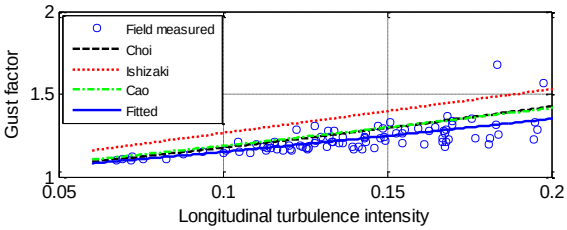

(b) Variation of gust factor with turbulence intensity

Fig. 11 Variation of gust factor with mean wind velocity and turbulence intensity

3.4 Gust factor

The gust factor is defined as the ratio of the gust speed within gust duration t_g (normally 3s) to the 10-minite mean wind speed, as follows

$$G_u(t_g) = 1 + \frac{max(\overline{u(t_g)})}{\overline{U}}, \quad G_v(t_g) = \frac{max(\overline{v(t_g)})}{\overline{U}} \tag{5}$$

where $max(\overline{u(t_g)})$ and $max(\overline{v(t_g)})$ are the maximum mean wind speed during t_g in longitudinal and lateral directions.

Fig. 11(a) shows the variations of the longitudinal gust factor with the 10-minite mean wind speed. It can be seen that the longitudinal gust factor gradually decreases with the increase of the mean wind speed and approaches a constant as the wind speed becomes larger. The mean longitudinal gust factor is 1.23 and is lower than the value (= 1.50) used in the current design codes and standards in China (GB 50009 2012) and the value (= 1.60) estimated by Cao *et al.* (2009) during Typhoon Maemi. The relationship between gust factor and turbulence intensity for typhoon has been studied for many years. Based on the studies of Ishizaki (1983), Choi (1983) and Cao *et al.* (2009), the empirical relationship between the gust factor and turbulence intensity is given as follows

$$G(t)=1+\mathrm{k}_1 I_u^{k_2}\, ln\frac{T_0}{t_g} \tag{6}$$

where k_1 = 0.5, k_2 = 1.0 are given in the Ishizaki's work (Ishizaki 1983), k_1 = 0.62, k_2 = 1.27 in Choi's work (Choi 1983) and k_1 = 0.50, k_2 = 1.15 in Cao's work (Cao *et al.* 2009); T_0 is the averaging time of the mean wind speed and t_g is the averaging time of the maximum peak gust. Fig. 11(b) shows the dependence of gust factor on turbulence intensity, with the empirical expressions of Ishizaki, Choi and Cao shown together. A fitting based on least-squares method yields k_1 = 0.47 and k_2 = 1.21. The Ishizaki's formula is estimated from the recorded data at the height of 15 m on Tarama Island and at the height of 30.8 m at Nakagawa. Cao's formula is estimated from the recorded data at height of 15.9 m for ultrasonic anemometers and 15.0 m for vane anemometers during Typhoon Maemi. However, the fitting formula during Typhoon *Vincente* is estimated from the recorded data at height of 461 m, which is much larger than the heights for Ishizaki's formula and Cao's formula. Consequently, for the case of Typhoon *Vincente*, the three formulae overestimate the gust factors.

3.5 Turbulence integral length scales

The turbulence integral length scales are measures of the average size of the turbulent eddies of the flow. The two common methods for determining the length scale of turbulence are autocorrelation function integral method (Eq. (7)) and power spectral method (Eq. (8)) (Simiu and Scanlan 1996).

$$L_i^x = \frac{U}{\sigma^2}\int_0^\infty R_i(\tau)d\tau \quad (i = u, v, w) \tag{7}$$

$$L_i^x = US_i(0)/(4\sigma_i^2) \quad (i = u, v, w) \tag{8}$$

where $R_i(\tau)$ is the auto-covariance function of the wind speed fluctuation, $S_i(0)$ is the value of spectra for f = 0 and σ_i^2 is the variance of fluctuating wind speed.

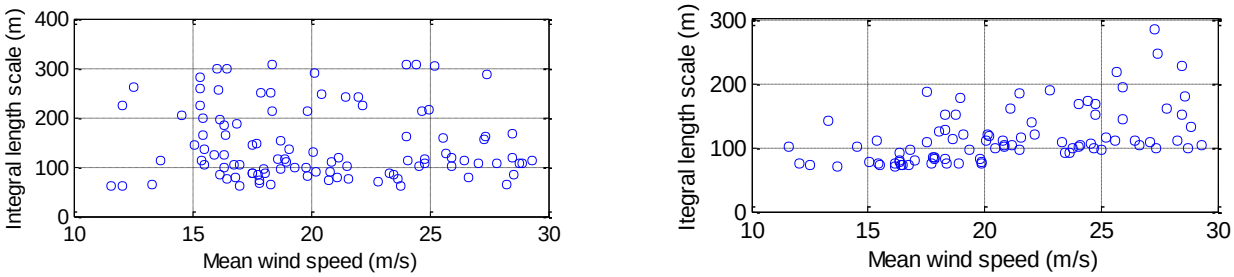

(a) Longitudinal (b) Lateral

Fig. 12 Variation of turbulence length scale with wind speed

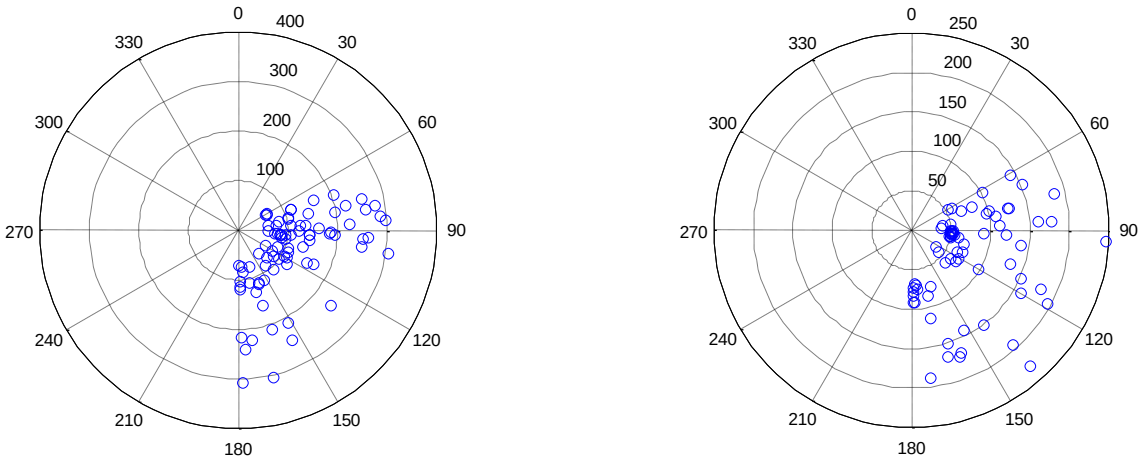

(a) Longitudinal (b) Lateral

Fig. 13 Variation of turbulence length scale with wind direction

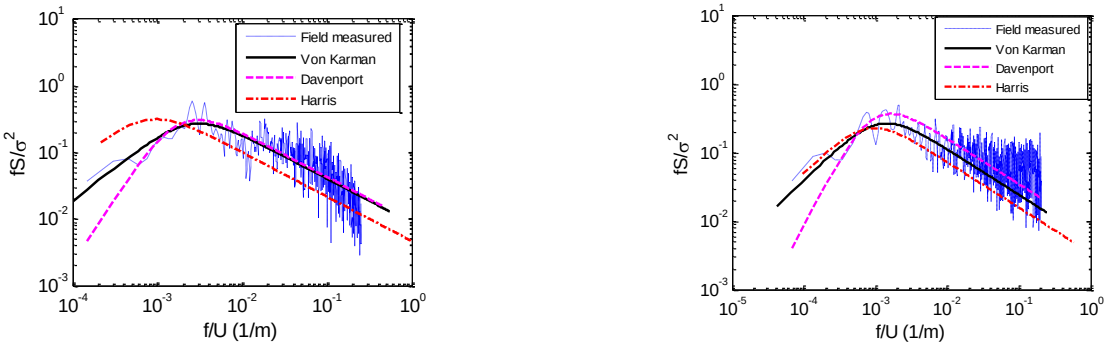

(a) U = 10.9 m/s (b) U = 24.0 m/s

Fig. 14 Normalized spectrum of longitudinal velocity component

Fig. 12 shows the variation of turbulence integral length scale in the longitudinal and lateral directions. The average values of turbulence integral length scales are 145 m and 95 m for the longitudinal and lateral directions. According to the Code recommended by AIJ (1996), the turbulence integral length scale in longitudinal direction is given as L_u = 100 × (z/100)0.5 = 392 m. It is obvious that the result from this study is much smaller than the result estimated according to AIJ (1996). This can be attributed to the dense tall buildings around Canton Tower. The ratio between the average value of the turbulence integral length scale in longitudinal and lateral directions is L_u:L_v = 145:95 = 1:0.65, which is larger than the result (L_u:L_v = 1:0.25) reported by Solari and Piccardo (2001). The main reason for the discrepancies may be attributed to the different measurement height. In this study, the wind speed was measured atop Canton Tower (at height of 461 m), but the result provided by Solari and Piccardo was obtained near ground. The ratio obtained from this study is close to the result (L_u:L_v = 1:0.57) measured by at the top of CPT (Li *et al*. 2008).

The variation of turbulence integral length scale with wind direction is shown in Fig. 13. It can be seen that the turbulence integral length scale of longitudinal wind

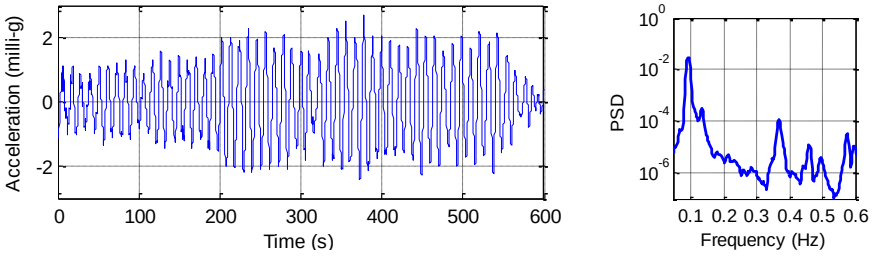

(a) X-direction

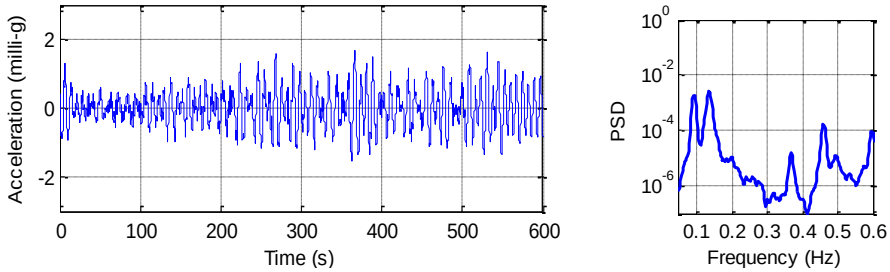

(b) Y-direction

Fig. 15 Acceleration at main tower top and their PSDs for U = 24 m/s

appears to be much larger when the wind direction is east, which may be attributed to the flat-water surface of Pearl River.

3.6 Wind spectra

Power spectral density function of fluctuating wind speed is used to describe the energy distribution of turbulence with frequency. In this study, two typical data with mean wind speed of 10.9 m/s and 24.0 m/s are analyzed. The normalized spectra of longitudinal velocity component for the two samples are shown in Fig. 14. Meanwhile, the Davenport spectra, Von Karman spectra and Harris spectra are also shown in Fig. 14. It can be seen from Fig. 14 that the fitted Davenport spectra is lower than the measured spectra at lower frequency range, but agrees well with measured spectra at high frequency range of interest for structural applications. The Harris spectrum exhibits large difference with the measured spectra, which is due to the fact that Harris spectrum does not reflect the variation of the spectra with height above ground. The Von Karman agrees well with measured spectra as the turbulence integral scale is used as free parameters for fitting.

4. Structural dynamic characteristics

4.1 Structural response

Twenty uni-axial accelerometers are installed at eight levels of the interior RC column, as shown in Figs. 3-4. Fig. 15 shows 10-minite X- and Y-direction accelerations at tower top and their PSDs for a mean wind velocity of 24 m/s with wind direction of 160° which is nearly perpendicular to X-direction.

The peak factors of acceleration response, defined as the ratio of peak acceleration to RMS value, in X- and Y-directions during Typhoon *Vincente*, are shown in Fig. 16. Partially due to the smaller stiffness in X-direction, the additional X-direction aerodynamic forces caused by vortex shedding may also intensify X-direction acceleration responses. The mean values of the peak response factors are 2.66 and 2.93 for X- and Y-directions responses, respectively. The theoretical peak factors for vortex-induced vibration and gust-induced buffeting are approximately 1.4 and 3.5 for the towers, respectively. Therefore, the measured responses appear to be a result of gust-induced buffeting and vortex-induced vibrations. A typical X-

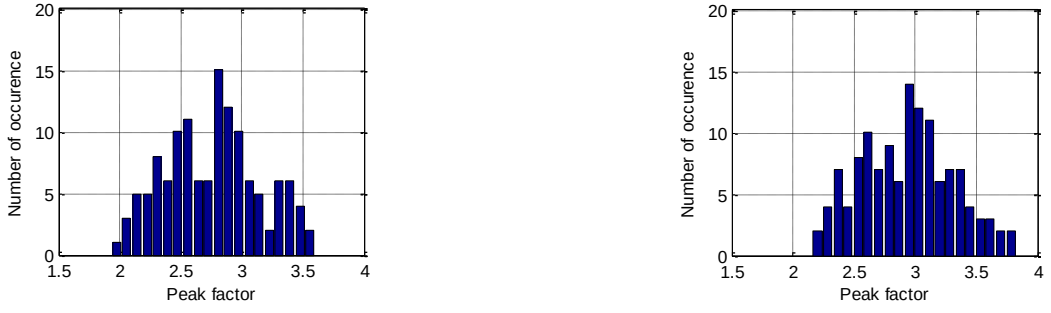

(a) X-direction (b) Y-direction

Fig. 16 Peak response factors for acceleration

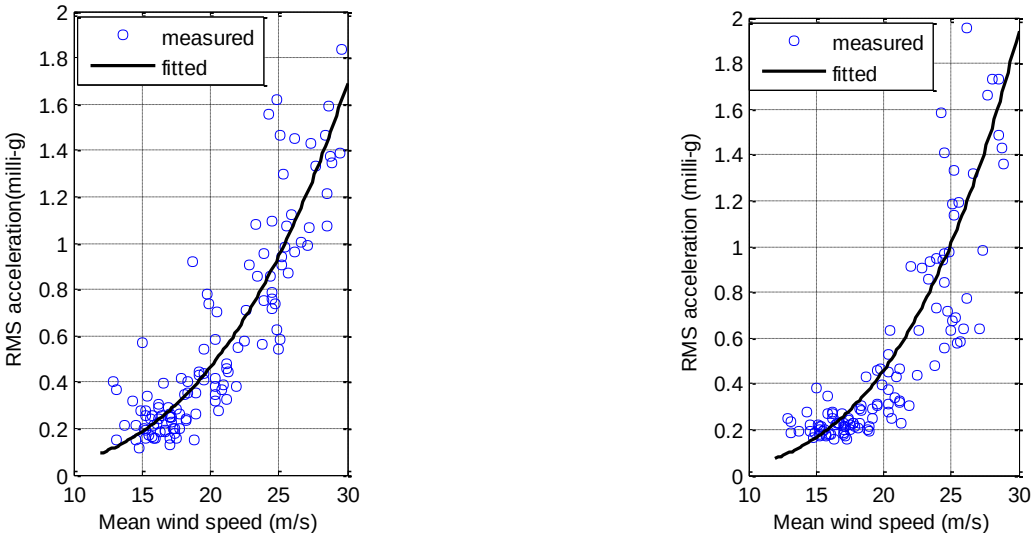

(a) X-direction (b) Y-direction

Fig. 17 Variation of acceleration responses with mean wind velocity

direction (crosswind) acceleration characterized by single-mode vibration is given in Fig. 15(a). For alongwind response in Y-direction as shown in Fig. 15(b), the response behaves like random vibrations, as it is contributed by the first two modes in each direction. However, wind tunnel tests of the Canton Tower show that wind-induced response is mainly a buffeting one. The deviation of wind tunnel tests from field measurements may be caused by Reynolds number effect, because the flow around the bluff body may be laminar for small Reynolds number of several hundred correspondents to the scaled model, which otherwise may be turbulent with regular shedding from full-scale body for larger Reynolds number. As mentioned above, the measured turbulence intensity may be less than the design values, which can further intensify the vortex-induced vibrations in full scale.

The variations of RMS of Y-direction and X-direction accelerations with mean wind velocity at a height of 446.8 m are shown in Fig. 17. It is noted that the acceleration responses increase as the wind speed increases. For the data presented in Fig. 17, the regression curves of acceleration response for each direction are expressed by

$$\sigma_Y = 3.39 \times 10^{-5} \bar{U}^{3.18} \tag{9}$$

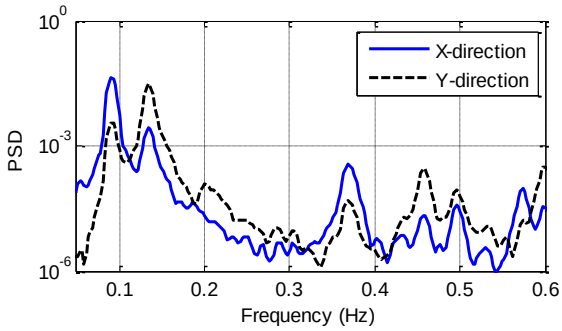

Fig. 18 PSD of 10-minute acceleration responses in X-direction and Y-direction

$$\sigma_X = 1.08 \times 10^{-5} \bar{U}^{3.55} \tag{10}$$

where σ_Y and σ_X are RMS of Y-direction and X-direction accelerations.

From Eqs. (9)-(10), the RMS acceleration for design wind velocity 52.4m/s are predicted as 10.0 milli-g in X-direction and 13.7 milli-g in Y-direction. During the wind tunnel tests, the RMS acceleration responses in X-direction and Y-direction for mean wind speed of 52.4m/s are 5.00

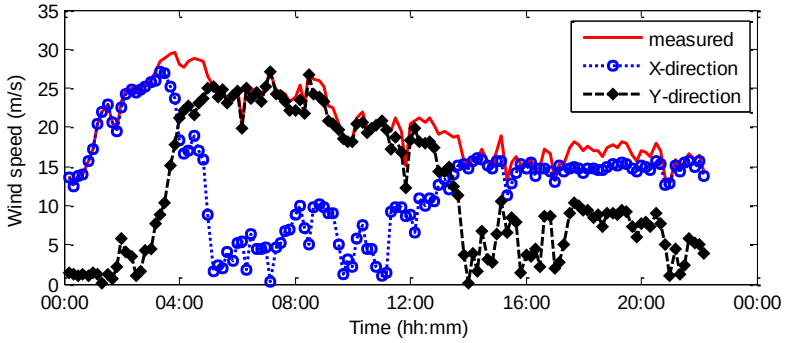

Fig. 19 Decomposed wind components in X-direction and Y-direction

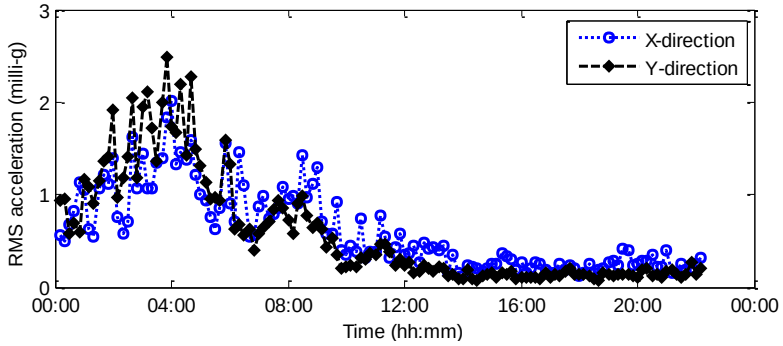

Fig. 20 RMS acceleration varied with time

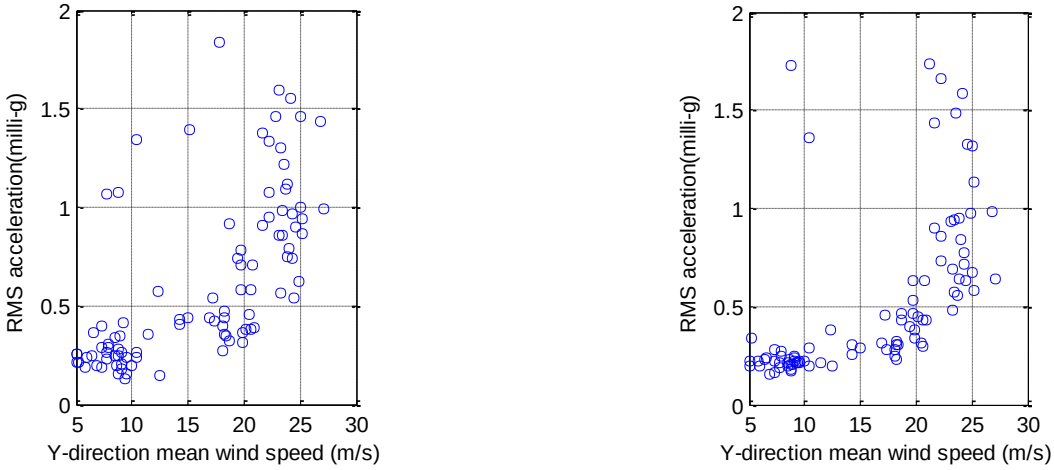

(a) In X-direction (b) In Y-direction

Fig. 21 Relationship between the Y-direction wind speed and RMS accelerations

milli-g and 4.00 milli-g, respectively. The total damping ratio is about 2% during wind tunnel tests, comprising aerodynamic damping about 0.3%, but is less than 1% during full scale tests, which results in the discrepancy of RMS acceleration.

Fig. 18 is the PSD of 10-minute acceleration responses in X-direction and Y-direction. This figure indicates that the vibration modes of the tower are coupled in the two directions, but the coupling is not strong. The wind-induced vibration of the tower in X-direction is mainly dominated by the first X-direction mode and, the dynamic response in Y-direction is mainly dominated by the first Y-direction mode.

To further study the characteristics of the wind-induced vibration, the measured wind is decomposed into X-direction component and Y-direction component, as shown in Fig. 19, and the RMS accelerations varied with time is shown in Fig. 20. Fig. 21 shows the relationship between the Y-direction wind speed and RMS accelerations. It can be seen that the RMS accelerations in X-direction show an obvious hump when the Y-direction wind speed is in the range from 20 m/s to 25 m/s, which seems to be the 'lock-in' phenomenon of the vortex-induced vibration.

One way to combine the accelerations from two orthogonal motions is to take the square root of the sum of the squares, as follows

$$\sigma = \sqrt{{\sigma_y}^2 + {\sigma_x}^2} \tag{11}$$

The resultant acceleration responses, which are plotted as function of mean wind speed and mean wind direction, are shown in Fig. 22. It is noted that the effect of magnitude of wind speed on the resultant responses is more significant than the wind direction.

For modern flexible tall buildings, especially such as Canton Tower, serviceability issues are of paramount importance and occupant comfort is a major concern in the design. It has been widely recognized that building acceleration is the most appropriate response component for checking the structural serviceability requirements under wind action. From Fig. 22, the maximum RMS acceleration is 3.1 milli-g (0.031 m/s^2) and the corresponding maximum 10-minite wind speed is 30.2 m/s.

International Standard Organization (ISO 1984) considers the relationship of structural frequency with the occupant comfort, and suggests that the acceleration criterion for a 5-year return period for building structures is

$$a_{rms} = 0.026 \times {f_1}^{-0.41} \tag{12}$$

where a_{rms} is the RMS acceleration (m/s^2), f_1 is the first structural frequency (Hz). Considering the reduction factor

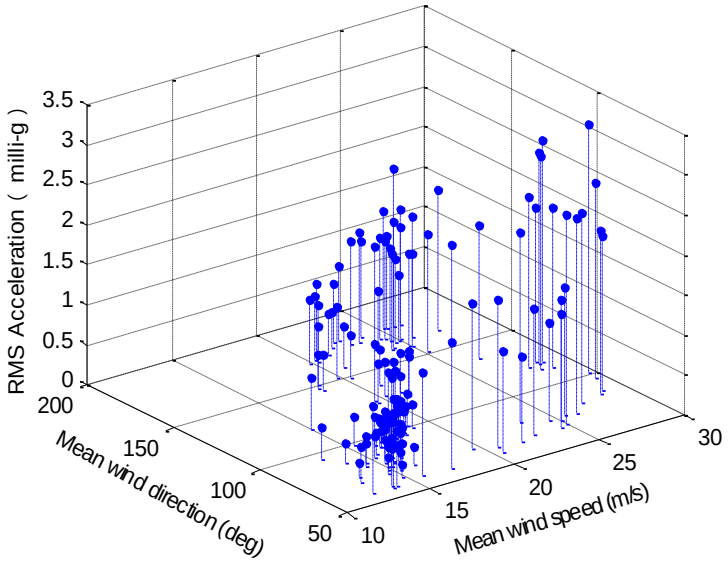

Fig. 22 Variation of acceleration with mean wind speed and wind direction

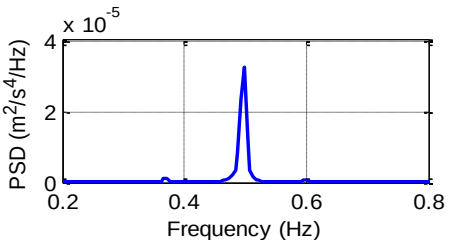

Fig. 23 PSD of torsional acceleration response at tower top

(0.72), Eq. (12) may be taken as acceleration criterion for a 1-year return period. It is calculated that the peak acceleration response should not be larger than 0.069 m/s^2 for a 5-year return period and 0.05 m/s^2 for a 1-year return period, respectively. However, the measured maximum acceleration is 0.031 m/s^2, which is lower than the acceleration criterion stated in ISO.

Table 1 Comparison of natural frequencies between measurement and prediction

Mode No.	Present study (Hz)	FEM (Hz)	Guo's Results (Hz)	Mode shape
1st	0.0928	0.095	0.0920	along X axis
2nd	0.1367	0.139	0.1361	along Y axis
3th	0.3711	--	0.3739	along X axis
4th	0.4590	--	0.4634	along Y axis
5th	0.4980	0.452	0.4996	torsion

4.2 Modal frequencies and mode

The power spectral densities (PSD) of a 10-minite acceleration data in X and Y directions are shown in Fig. 18. The PSD of torsional acceleration is derived from the difference of the two accelerations in Y direction at height

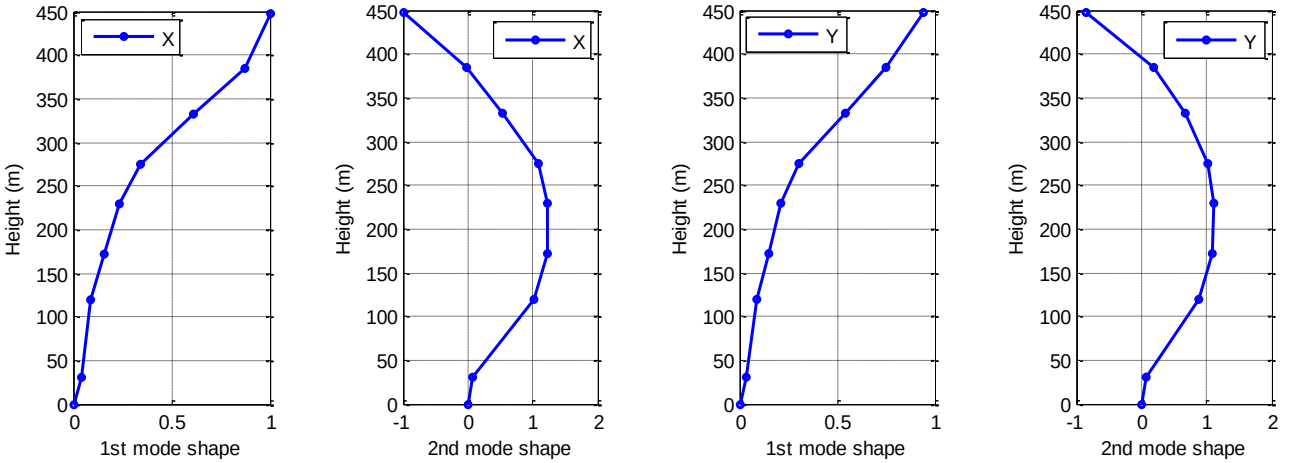

(a) 1st mode in X direction (b) 2nd mode in X direction (c) 1st mode in Y direction (d) 2nd mode in Y direction

Fig. 24 First four bending mode shapes

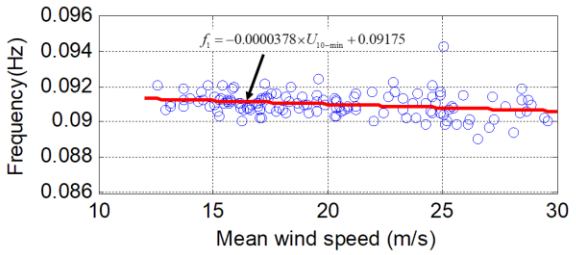

(a) 1st mode

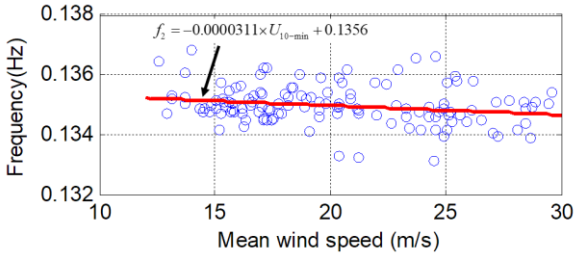

(b) 2nd mode

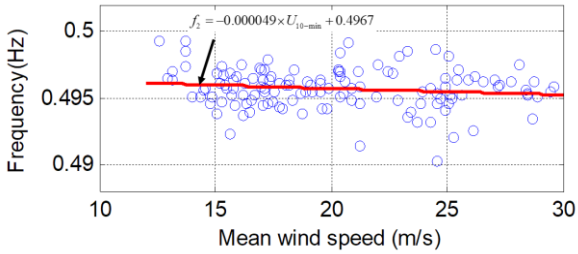

(c) 5th mode

Fig. 25 Natural frequency versus mean wind speed

of 446.8 m and is shown in Fig. 23. Table 1 gives the modal frequencies identified by peak-picking method, along with analytical prediction from finite element model and the experimental modal parameters during Typhoon Sarika (Guo *et al*. 2012). The experimental results are in good agreement with the results measured during Typhoon Sarika, and the difference between experimental results and finite element model prediction is also very small for the first two modes. However, there is some difference in modal frequency for the torsional mode.

The experimental mode shapes for the first two modes in X and Y directions are shown in Fig. 24. It can be seen that the largest displacement is at the tower top for the 1st mode shape and is at the tower waist for 2nd mode shape in both directions. The correlation of mode shapes between measurement and finite element analysis are larger than 0.95.

Due to the effect of aerodynamic stiffness from wind flow and possible contribution of non-structural component, the measured frequency may vary with wind velocity. In this study, the variation of natural frequencies f_i with wind velocity for the 1st, 2nd and 5th modes are shown in Fig. 25. A linear regression model is used to model the relationship, as

$$f_i = a_1 \times \bar{U} + a_2 \tag{13}$$

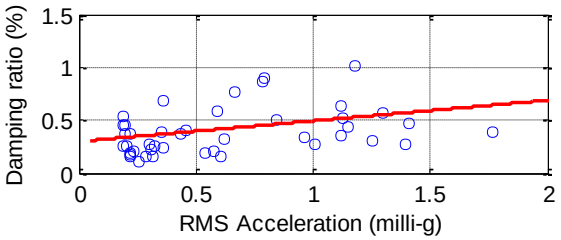

(a) Damping ratio of 1st mode identified from X direction

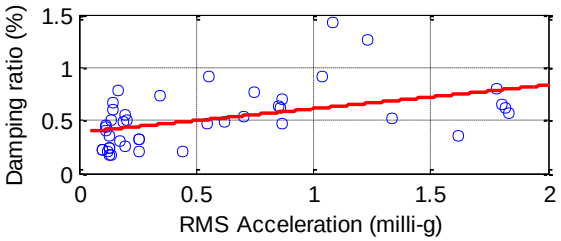

(b) Damping ratio of 1st mode identified from Y direction

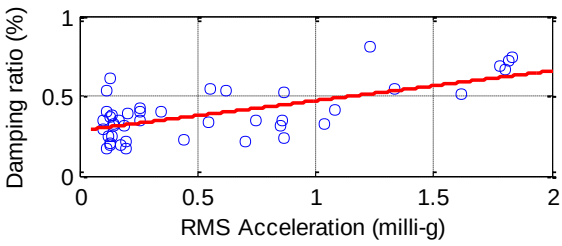

(c) Damping ratio of 2nd mode identified from X direction

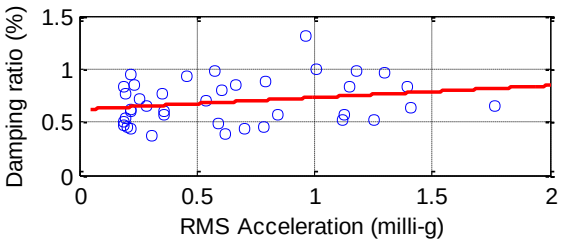

(d) Damping ratio of 2nd mode identified from Y direction

Fig. 26 Identified damping ratio versus vibration amplitude

where a_1 and a_2 are the regression coefficients. The fitted lines are also given in Fig. 25. The identified natural frequencies for those three modes show a very slight decreasing trend with wind velocity. However, it is seen that the change in modal frequency with wind velocity is rather insignificant.

4.3 Damping ratio

Structural damping is an important parameter for evaluating dynamic responses of wind-sensitive structures. Damping ratios used for structural design which is often based on past practice does not always agree with those of the actual structures. Many measurements for structural damping have been made throughout the world (Kareem and Gurley 1996, Tamura and Suganuma 1996). While forced vibration method where a structure is excited into resonance by external exciters is the most reliable way to identify damping ratios (Ellis 1996), lack of apparatus

capable of exciting such mega structure prevents its real applications. In this study, ambient vibration data under typhoon is used.

The accelerations measured at the height of 446.8 m are used to identify the damping ratios. The random decrement technique (RDT) is employed to evaluate the damping ratio, which is recognized as a quick and practical method for identifying damping ratio. In order to improve identification accuracy, the measured accelerations of the 30-minute duration rather than the 10-minite duration are adopted. The acceleration data are band-pass filtered to remove the components that are not concerned. The variations of the identified damping ratios with RMS values of accelerations for the first two modes in X and Y directions are shown in Fig. 26, where a linear least-squared fitting is also given. Despite that the scatter in identified damping ratio, general observations can be obtained. First, at low vibration amplitude, namely at low wind speed, the damping ratio identified is as low as 0.2%~0.4% critical damping, which indicates that lower structural damping is possible for high-rise concrete buildings. Second, it is seen that the identified damping ratio increases when the RMS accelerations increase for the vibration modes in both directions. For high wind velocity, the vibration modes in the alongwind direction (Y-direction) seem to have larger damping ratios that the vibration modes in the crosswind direction, which is consistent with the quasi-steady theory. Third, the increasing rate of damping ratio becomes smaller at high wind velocity for the first mode, which can be explained that the structural damping is saturated after a critical vibration amplitude. The half-power bandwidth (HPBW) is also used to identify the damping ratio and the results are listed in Table 2. The damping ratio for the 1st mode identified from the acceleration in the X direction is very close to that identified from the acceleration in the Y direction. When comparing the damping ratio identified by using RDT and HPBW, it is seen that the damping ratios have large variations.

Table 2 Damping ratio identified by half power bandwidth (HPBW) (U = 18.2 m/s)

Mode	X-direction		Y-direction	
1st	Acc 17	Acc 18	Acc 17	Acc 18
2nd	1.49%	1.49%	1.49%	1.49%

4.4 Displacement responses

To monitor the displacements of the tower under wind actions, a bi-axial tiltmeter is installed at the height of 443.6 m, which can measure the tilt in the X and Y directions synchronously. As a first approximation, the horizontal displacements can be obtained as

$$D = H \times sin(\theta) \tag{14}$$

where H is the height of tiltmeter above ground; θ is the measured inclination angle.

Fig. 27 shows the calculated time histories of horizontal

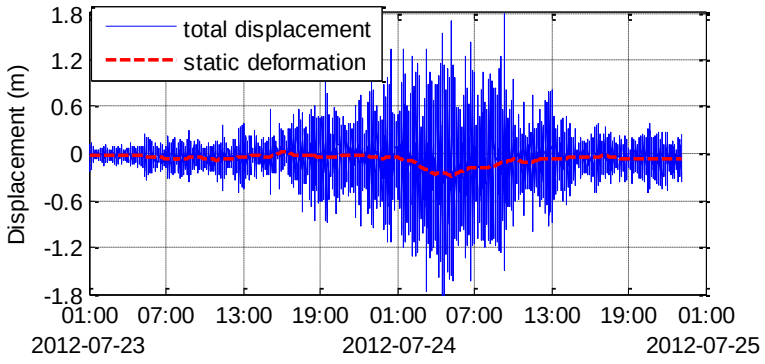

(a) X-direction

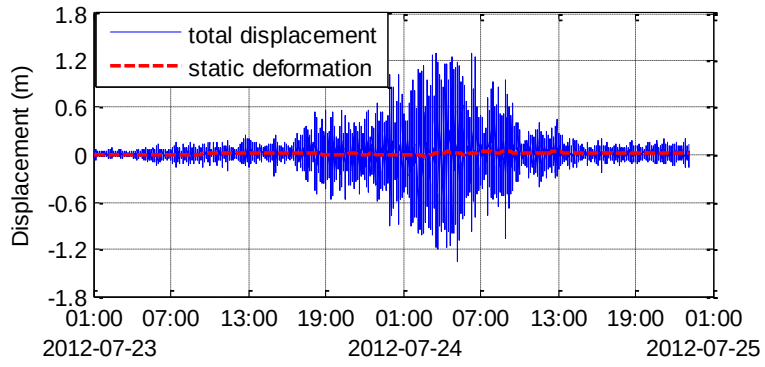

(b) Y-direction

Fig. 27 Time histories of displacements

displacements during Typhoon *Vincente* in X and Y directions. The static deformations in X and Y directions are estimated from the calculated time histories of horizontal displacements, also shown in Fig. 27. The displacements in both directions started to increase gradually at night on 23 July, reaching the peaks at about 4:00 am on 24 July, then they began to decrease, which is consistent with the wind velocity. The trend of the static deformation is also consistent with the wind velocity.

The PSDs of horizontal displacements in X and Y directions are shown in Fig. 28. The first two modal frequencies identified from the PSD of displacements are 0.092 Hz and 0.137 Hz, which shows a good agreement with those identified from the PSD diagram of acceleration data. Fig. 29 shows the relationship between the RMS displacement and measured mean wind speed. It is clear that the RMS displacement increases when the wind speed increases.

Fig. 30 shows the relationships between Y-direction wind speeds and RMS displacements. Comparing with Fig. 21, the relationships between wind speeds and displacement responses coincide with that between wind speeds and acceleration responses. The results further verify that the tower appears to suffer from vortex-induced vibration when the wind speed in Y-direction is in the range from 20 m/s to 25 m/s.

The relationship between the 10-minite mean static deformation and the mean wind speed is studied. Assuming that the static deformation is proportional to the square of wind speed, the predicted tower top static deformations at the design wind speed of 52.4 m/s are 0.748 m and 0.494 m for the X direction and the Y direction, respectively. The comparison of the predicted static deformation with the measured static deformation is given in Fig. 31. In the X direction, the predicted values are close to the measured ones. In the Y-direction, static deformation is overestimated.

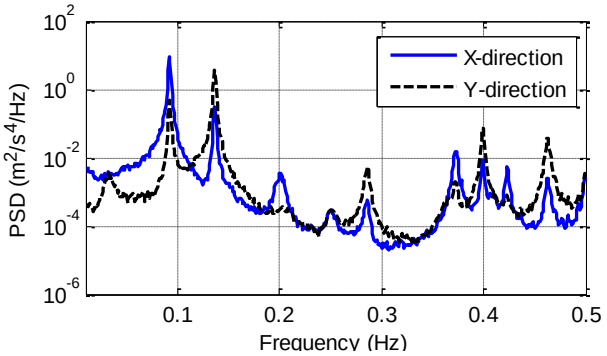

Fig. 28 PSD of displacements ($\bar{U}$ = 15.3 m/s)

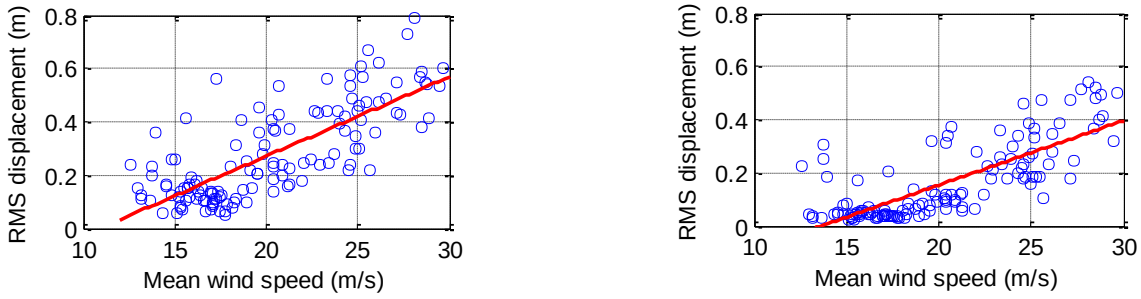

(a) X direction (b) Y direction

Fig. 29 Variation of RMS displacements with mean wind speed

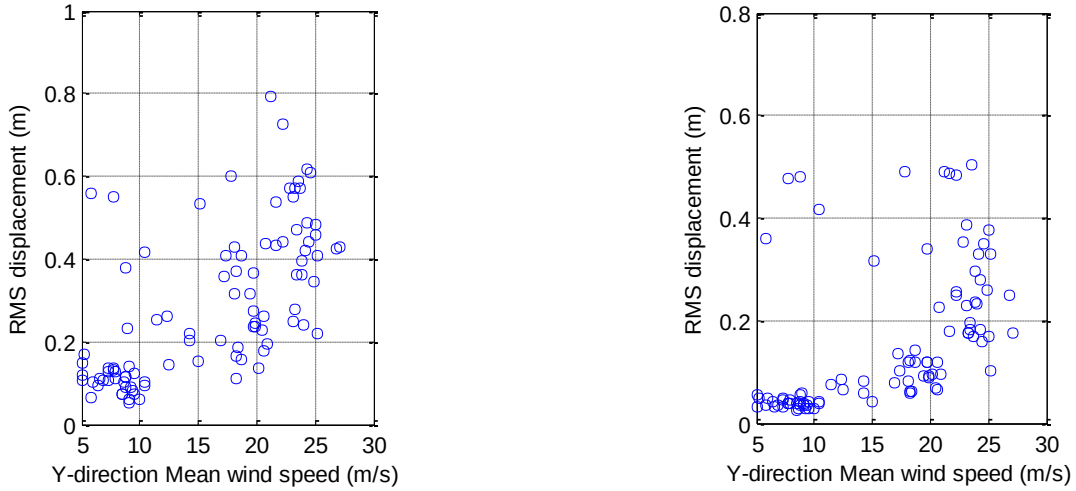

(a) X direction (b) Y direction

Fig. 30 Relationship between the Y-direction wind speed and RMS accelerations

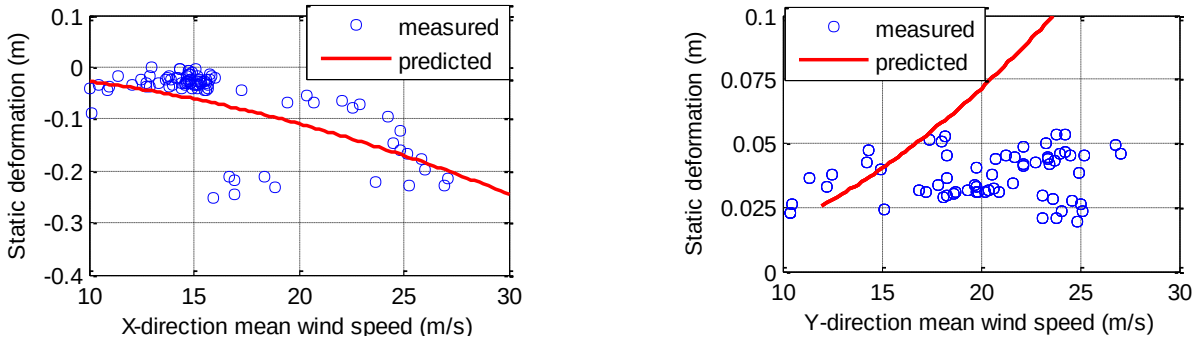

(a) X direction (b) Y direction

Fig. 31 Variation of 10-minite static deformation with wind speed

5. Conclusions

The wind characteristics and structural responses measured at the Canton tower during Typhoon *Vincente* are analyzed. For wind at 461 m above ground (upper level of atmospheric boundary layer), the alongwind wind spectra can be well described by auto-spectra of the Von Karman and Davenport type. The measured average longitudinal turbulent intensity seems to slightly larger than the nominal value adopted in design; however it can be smaller than the nominal value which implies that the wind tunnel testing may underestimate the crosswind structural responses for certain lock-in velocity range of vortex shedding.

Analyses of peak factors and power spectral density in acceleration responses indicate that the crosswind structural responses are a combination of gust-induced buffeting and vortex-induced vibrations for some wind directions, which seems to be not predicted by wind tunnel tests. Modal frequencies and mode shapes identified during different typhoon events are quite close to each other, and are also close to those from finite element prediction except for the torsional mode. Modal damping ratios identified at lower amplitude of vibration are 0.2%~0.4% of critical, and the variation of modal damping with vibration amplitude is obvious, which is mainly caused by aerodynamic damping. On the other hand, the change of modal frequency with wind velocity seems insignificant. During the Typhoon *Vincente*, the maximum acceleration responses are well within the serviceability limit.

Acknowledgments

This study is sponsored by the National Science Foundation of China (project No. 51422806; 51708208). The authors also thank Prof. Y.Q. Ni at the Hong Kong Polytechnic University for providing the measurement data of Canton tower.

References

AIJ 1996 (1996), AIJ Recommendations for Loads on Buildings, Architectural Institute of Japan; Tokyo, Japan.

ASCE7-05 (2006), Minimum Design Loads for Buildings and Other Structures-ASCE, American Society of Civil Engineers (ASCE); New York, USA.

Au, S.K., Zhang, F.L. and To, P. (2012), "Field observations on modal properties of two tall buildings under strong wind", *J. Wind Eng. Ind. Aerod.*, **101**, 12-23. https://doi.org/10.1016/j.jweia.2011.12.002

Ballio, G., Maberini, F. and Solari, G. (1992), "A 60-year old, 100m high steel tower: limit states under wind action", *J. Wind Eng. Ind. Aerod.*, **43**(1-3), 2089-2100. https://doi.org/10.1016/0167-6105(92)90639-R

Banks, D. and Meroney, R.N. (2001), "The applicability of quasi-steady theory to pressure statistics beneath roof-top vortices", *J. Wind Eng. Ind. Aerod.*, **89**, 569-598. https://doi.org/10.1016/S0167-6105(00)00092-1

Bashor R. Bobby S., Kijewski-Correa T. and Kareem A. (2012), "Full-scale performance evaluation of tall buildings under wind", *J. Wind Eng. Ind. Aerod.*, **104**, 88-97. https://doi.org/10.1016/j.jweia.2012.04.007

Bortoluzzi, D., Casciati, S., Elia, L. and Faravelli, L. (2015), "Design of a TMD solution to mitigate wind-induced local vibration in an existing timber footbridge", *Smart Struct. Syst., Int. J.*, **16**(3), 459-478. https://doi.org/10.12989/sss.2015.16.3.459

Brownjohn, J.M. (2007), "Structural health monitoring of civil structures", *Philosoph. Transact.: Series A: Mathe., Phys., Eng. Sci.*, **365**(1851), 589-622.

Brownjohn, J.M. and Pan, T.C. (2008), "Identifying loading and response mechanisms from ten years performance monitoring of a tall building", *J Perform. Constr. Fac.*-ASCE, **22**, 24-34. https://dx.doi.org/10.1061/(ASCE)0887-3828(2008)22:1(24)

Campbells, S., Kwok, K.C.S. and Hitchock, P.A. (2005), "Dynamic characteristics and wind-induced response of two high-rise residential buildings during typhoons", *J. Wind Eng. Ind. Aerod.*, **93**(6), 461-482. https://dx.doi.org/10.1016/j.jweia.2005.03.005

Cao, S.Y., Tamura, Y., Kikuchi, N., Saito, M., Nakayama, I. and Matsuzaki, Y. (2009). "Wind characteristics of a strong typhoon", *J. Wind Eng. Ind. Aerod.*, **97**(1), 11-21. https://doi.org/10.1016/j.jweia.2008.10.002

Caracoglia, L. and Jones, N.P. (2009), "Analysis of full-scale wind and pressure measurements on a low-rise building", *Eng. Struct.*, **97**(5-6), 157-173. https://dx.doi.org/10.1016/j.jweia.2009.06.001

Chen, W.H., Lu, Z.R. and Lin, W. (2011), "Theoretical and experimental modal analysis of the Guangzhou New TV Tower". *Eng. Struct.*, **33**(12), 3628-3646. https://doi.org/10.1016/j.engstruct.2011.07.028

Choi, C.K. (1983), Wind loading in Hong Kong: commentary on the code of practice on wind effects Hong Kong, Hong Kong Institute of Engineers, Hong Kong, China.

Davenport, A.G. (1962), "The Spectrum of horizontal gustiness

near the ground in high winds", *Q. J. Roy. Meteor. Soc.*, **87**, 194-211. https://doi.org/10.1002/qj.49708837618

Davenport, A.G. (1975), "Perspectives on the full-scale measurement of wind effect", *J. Wind Eng. Ind. Aerod.*, **1**(1), 23-54. https://doi.org/10.1016/0167-6105(75)90005-7

Ellis, B.R. (1996), "Full-scale measurements of dynamic characteristics of buildings in UK", *J. Wind Eng. Ind. Aerod.*, **59**(2-3), 365-382. https://doi.org/10.1016/0167-6105(96)00017-7

Fu, J.Y., Li, Q.S. and Wu, J.R. (2008), "Field measurements of boundary layer wind characteristics and wind-induced responses of super-tall buildings", *J. Wind Eng. Ind. Aerod.*, **96**(8-9), 1332-1358. https://doi.org/10.1016/j.jweia.2008.03.004

GB 50009 (2012), Load Code for the design of building structures, Beijing, Ministry of Housing and Urban-Rural Development of the People's Republic of China (MOHURD); Beijing, China.

Guo, Y.L., Kareem, A., Ni, Y.Q. and Liao, W.Y. (2012), "Performance evaluation of Canton Tower under winds based on full-scale data", *J. Wind Eng. Ind. Aerod.*, **104-106**, 116-128. https://doi.org/10.1016/j.jweia.2012.04.001

Harris, R.I. (1968), "On the spectrum and auto-correlation function of gustiness in high winds", An E.R.A. technical report no.5273; Electrical Research Association.

He, Y., Han, X., Li, Q.S., Zhu, H.P. and He, Y. (2018), "Monitoring of wind effects on 600 m high Ping-An Finance Center during Typhoon Haima", *Eng. Struct.*, **167**, 308-326. https://dx.doi.org/10.1016/j.engstruct.2018.04.021

Holmes, J.D. (2001), Wind Loadings of Structures, Spon Press, Taylor & Francis Group, Australia.

Hong Kong Observatory (2012), An overview of tropical cyclones in July 2012; Hong Kong Observatory, Hong Kong, China. http://gb.weather.gov.hk/informtc/tc2012/tc1207c_uc.htm

Irwin, P.A. (2008), "Bluff body aerodynamics in wind engineering", *J. Wind Eng. Ind. Aerod.*, **96**(6-7), 701-702. https://doi.org/10.1016/j.jweia.2007.06.008

Irwin, P.A. (2009), "Wind engineering challenges of the new generation of super-tall buildings", *J. Wind Eng. Ind. Aerod.*, **97**(7-8), 328-334. https://doi.org/10.1016/j.jweia.2009.05.001

Ishizaki, H. (1983), "Wind profiles, turbulence intensities and gust factors for design in typhoon-prone regions", *J. Wind Eng. Ind. Aerod.*, **13**(1-3), 55-66. https://doi.org/10.1016/0167-6105(83)90128-9

ISO6897 (1984), Guidelines for the evaluation of the response of occupants of fixed structures, especially buildings and off-shore structures, to low-frequency horizontal motion (0.063 to 1Hz), ISO.

Jeary, A.P. (1992), "Establishing non-linear damping characteristics of structures from non-stationary time-histories", *The Structural Engineer*, **70**(4), 62-66. http://www.istructe.org/webtest/files/8b/8bb58868-a1b8-4dc7-892a-f258b311ee53.pdf

Kareem, A. and Gurley, K. (1996), "Damping in structures: its evaluation and treatment of uncertainty", *J. Wind Eng. Ind. Aerod.*, **59**(2-3), 131-157. https://doi.org/10.1016/0167-6105(96)00004-9

Kareem, A., Kijewski, T. and Tamura, Y. (1999), "Mitigation of motions of tall buildings with specific examples of recent applications", *Wind Struct., Int. J.*, **2**(3), 201-251. https://doi.org/10.12989/was.1999.2.3.201

Kijewski-Correa, T., Kilpatrick, J. and Kareem, A. (2006), "Validating wind-induced response of tall buildings: Synopsis of the chicago full-scale monitoring program", *J. Struct. Eng.*, **132**(10), 1509-1523. https://dx.doi.org/10.1061/(ASCE)0733-9445(2006)132:10(1509)

Li, Q.S., Xiao, Y.Q., Wong, C.K. and Jeary, A.P. (2004), "Field measurements of typhoon effects on a super tall building", *Eng. Struct.*, **26**(2), 233-244. https://doi.org/10.1016/j.engstruct.2003.09.013

Li, Q.S., Xiao, Y.Q., Wu, J.R., Fu, J.Y. and Li, Z.N. (2008), "Typhoon effects on super-tall buildings", *J. Sound Vib.*, **313**(3-5), 581-602. https://doi.org/10.1016/j.jsv.2007.11.059

Lu, Z., Wang, D.C., Masri, S.F. and Lu, X.L. (2016), "An experimental study of vibration control of wind-excited high-rise buildings using particle tuned mass dampers", *Smart Struct. Syst., Int. J.*, **18**(1), 93-115. https://doi.org/10.12989/sss.2016.18.1.093

Ni, Y.Q., Xia, Y., Liao, W.Y. and Ko, J.M. (2009), "Technology innovation in developing the structural health monitoring system for Guangzhou New TV Tower", *Struct. Control Hlth.*, **16**(1), 73-98. https://doi.org/10.1002/stc.303

Porterfield, M. and Jones, N.P. (2001), "Development of a field measurement instrumentation system for low-rise construction", *Wind Struct., Int. J.*, **4**(3), 247-260. https://doi.org/10.12989/was.2001.4.3.247

Simiu, E. and Scanlan, R.H. (1996), *Wind Effects on Structures* (Third Edition), A Wiley-inter science publication, New York, USA.

Siringoringo, D.M. and Fujino, Y. (2017), "Wind-induced responses and dynamic characteristics of an asymmetrical base-isolated building observed during typhoons", *J. Wind Eng. Ind. Aerod.*, **167**, 183-197. https://doi.org/10.1016/j.jweia.2017.04.020

Solari, G. and Piccardo, G. (2001), "Probabilistic 3-D turbulence for gust buffeting of structures", *Probabil. Eng. Mech.*, **16**(1), 73-86. https://doi.org/10.1016/S0266-8920(00)00010-2

Sun, H.X., Zuo, L., Wang, X.Y., Peng, J. and Wang, W.X. (2019), "Exact H_2 optimal solutions to inerter-based isolation systems for building structures", *Struct. Control Hlth.*, **26**(6), 1-21. https://doi.org/10.1002/stc.2357

Tamura, Y. and Suganuma, S. (1996), "Evaluation of amplitude-dependent damping and natural frequency of buildings during strong winds", *J. Wind Eng. Ind. Aerod.*, **59**(2-3), 115-130. https://doi.org/10.1016/0167-6105(96)00003-7

Tamura, Y., Yoshida, A., Ishibashi, R., Matsui, M. and Pagnini, L.C. (2002), "Measurement of wind-induced response of buildings using RTK-GPS and integrity monitoring", *The Second International Symposium on Advances in Wind and Structures* (*AWAS'02*), Busan, Korea, August.

Tao, T.Y., Wang, H. and Li, A.Q. (2016), "Stationary and non-stationary analysis on the wind characteristics of a tropical storm", *Smart Struct. Syst., Int. J.*, **17**(6), 1067-1085. https://doi.org/10.12989/sss.2016.17.6.1067

Von Karman, T. (1948), "Progress in the statistical theory of turbulence", *Proceedings of the National Academy of Sciences of the United States of America*, **34**(11), 530-539. https://dx.doi.org/10.1073%2Fpnas.34.11.530

Xu, Y.L. and Zhan, S. (2001), "Field measurements of Di Wang Tower during Typhoon York", *J. Wind Eng. Ind. Aerod.*, **89**(1), 73-93. https://doi.org/10.1016/S0167-6105(00)00029-5

Ye, X.W., Yuan, L. and Xi, P.S. (2018), "SHM-based probabilistic representation of wind properties: statistical analysis and bivariate modeling", *Smart Struct. Syst., Int. J.*, **21**(5), 591-600. https://doi.org/10.12989/sss.2018.21.5.591

Zhang, J.W. and Li, Q.S. (2018), "Field measurements of wind pressures on a 600 m high skyscraper during a landfall typhoon and comparison with wind tunnel test", *J. Wind Eng. Ind. Aerod.*, **175**, 391-407. https://doi.org/10.1016/j.jweia.2018.02.012

Zhu, L.D., Ding, Q.S. and Chen, W. (2006), "Wind tunnel test of aeroelastic full model of Guangzhou New TV Tower. Report", State Key Laboratory of Disaster Reduction in Civil Engineering, Tongji University, China.

BS